

Exploiting Multipath Information for Integrated Localization and Sensing via PHD Filtering

Yinuo Du, Hanying Zhao, *Member, IEEE*, Yang Liu, Xinlei Yu, Yuan Shen, *Senior Member, IEEE*

Abstract

Accurate localization and perception are pivotal for enhancing the safety and reliability of vehicles. However, current localization methods suffer from reduced accuracy when the line-of-sight (LOS) path is obstructed, or a combination of reflections and scatterings is present. In this paper, we present an integrated localization and sensing method that delivers superior performance in complex environments while being computationally efficient. Our method uniformly leverages various types of multipath components (MPCs) through the lens of random finite sets (RFSs), encompassing reflections, scatterings, and their combinations. This advancement eliminates the need for the multipath identification step and streamlines the filtering process by removing the necessity for distinct filters for different multipath types, a requirement that was critical in previous research. The simulation results demonstrate the superior performance of our method in both robustness and effectiveness, particularly in complex environments where the LOS MPC is obscured and in situations involving clutter and missed detection of MPC measurements.

Index Terms

Integrated localization and sensing, multipath propagation environments, PHD filtering

Yinuo Du, Hanying Zhao and Yuan Shen are with the Department of Electronic Engineering, and Beijing National Research Center for Information Science and Technology, Tsinghua University, Beijing 100084, China (e-mail: duyn19@mails.tsinghua.edu.cn; {hying_zhao,shenyuan_ee}@tsinghua.edu.cn).

Yang Liu and Xinlei Yu are with the Department of Standards Research, OPPO Inc., Beijing 100101, China (e-mail: liuyangbj@oppo.com; xinleiyu@hotmail.com).

This work has been submitted to the *IEEE Transactions on Vehicular Technology* for possible publication. Copyright may be transferred without notice, after which this version may no longer be accessible.

I. INTRODUCTION

High-accuracy localization with environmental sensibility is a critical technology in autonomous driving and 6G communication systems [1]. However, achieving precise localization in complex propagation environments poses a significant challenge for vehicles, primarily due to obstructions, reflections, and signal scatterings, leading to interference and phase shifting of received signals. To bolster vehicle safety and reliability, it is essential to address these complexities in localization.

Conventional localization methods put great efforts into eliminating these effects to extract line-of-sight (LOS) multipath component (MPC) for positioning. Nowadays, with the development of wireless technologies such as vehicle-mounted large bandwidth and large-scale antenna arrays, the high temporal- and spatial-resolution measurements enable us to separate mixed signals and estimate both LOS and non-line-of-sight (NLOS) MPCs [2]. Therefore, there are a growing number of localization methods that aim to exploit these multipath information to improve localization accuracy and achieve environmental sensing [3]–[6]. This topic is often referred to as radio simultaneous localization and mapping (SLAM). We give a brief review of them and make a comparison between existing works and ours.

In [3], the authors use a monostatic UWB device to detect and localize surrounding features. They adopt particle filtering with two methods of associating measurements with landmarks: Nearest Neighbor Data Association and Probabilistic Data Association. In [6], the authors use an adaptive federal filter to handle NLOS MPCs. However, their approach is limited to a specific number of MPCs and only considers reflection MPCs. Channel-SLAM in [4] treats multipath components as signals emitted from virtual transmitters (VTs), and an Rao-Blackwellised particle filter (RBPF) based on Recursive Bayesian filtering is employed to improve computational tractability by sampling particles in a subspace. Other works such as [7], [8] achieve radio SLAM using reconfigurable intelligent surfaces (RISs), where Murty’s algorithm is adopted to handle data association in [7]. As these works have mentioned, one of the main challenges of radio-SLAM lies in data association, i.e., assigning measurements to corresponding landmarks. To address this issue, based on finite-set statistics (FISST), the random finite set (RFS) theory and probability hypothesis density (PHD) filtering are introduced in radio-SLAM, which group time-varying elements into RFSs, explicitly eliminates the complicated data association step, showcasing its great advantages compared with the traditional RBPF-SLAM methods [9]–[11]. The authors in [5] proposed a cooperative vehicle positioning and radio environment mapping

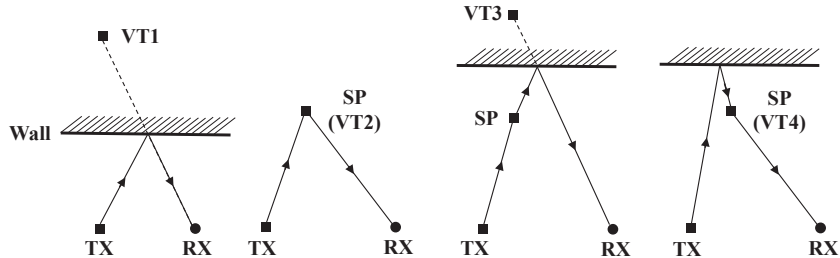


Fig. 1. An illustration to show the geometric relationships among transmitters (Txs), receivers (Rxs), and VTs for various MPCs: planar reflections (left), scattering points (SPs) (second from the left), and a combination of one scattering and one reflection (third and fourth from the left). The multipath signals can be visualized as if they were virtually emitted from VTs.

method via a multiple-model PHD filter. Although a promising performance is achieved, multiple PHD filters are derived and employed for different types of MPCs since MPCs originating from reflections and scatterings are treated distinctly. Moreover, this method fails to handle MPCs which are under the dual effect of scatterings and reflections.

In this paper, we present an integrated localization and sensing method that delivers superior performance in complex environments while being computationally efficient. Our method can uniformly leverage various types of MPCs, encompassing reflections, scatterings, and their combinations, thus bypassing the multipath identification step. The key enabler is the introduced MPC model represented as an RFS, which augments the state space to characterize the diverse geometric relationships between the agent and the environment for each MPC type. This advancement simplifies the filtering process by eliminating the requirement of separate filters for different types of MPCs, a step that was essential in previous studies like [5]. Our method offers more streamlined and versatile solutions for integrated localization and sensing in complex environments, which can serve as a practical guideline for implementation and advancement in areas such as autonomous driving and 6G.

II. SYSTEM MODEL

Consider a 2D localization scenario where a vehicle (agent) receives wireless signals transmitted from a static base station (anchor) for positioning.¹ Let $\mathbf{r}_b = [x_b \ y_b]^T$ denote the position

¹Our method is also applicable to 3D scenarios and multi-anchor systems. In 3D scenarios, it is adapted by adding elevation angles to the observation space and incorporating the z -axis into the state space. For multi-anchor systems, our approach is extended by augmenting observations from all anchors within the observation space.

of the stationary anchor. At time instant t_k with $k \in \mathbb{Z}^+$, the agent state can be described by

$$\mathbf{x}_k = \begin{bmatrix} \mathbf{r}_k^T & \mathbf{v}_k^T & b_k \end{bmatrix}^T \quad (1)$$

where $\mathbf{r}_k = [x_k \ y_k]^T$, $\mathbf{v}_k = [v_{x_k} \ v_{y_k}]^T$ and b_k denote position, velocity and ranging bias incurred by clock offset, respectively. At time $t_{k+1} := t_k + \Delta t$, the agent's new state yields:

$$\mathbf{x}_{k+1} = \mathbf{A}\mathbf{x}_k + \mathbf{B}\mathbf{n}_k \quad (2)$$

where $\mathbf{n}_k = [u_{x,k} \ u_{y,k} \ u_{b,k}]^T$ is the process noise modelled as additive white Gaussian noise (AWGN) with variances σ_x^2 , σ_y^2 and σ_b^2 . \mathbf{A} and \mathbf{B} are transition matrices, which can be obtained from $\mathbf{r}_{k+1} = \mathbf{r}_k + \mathbf{v}_k \Delta t + [u_{x,k} \ u_{y,k}]^T \Delta t^2 / 2$, $\mathbf{v}_{k+1} = \mathbf{v}_k + [u_{x,k} \ u_{y,k}]^T \Delta t$, and $b_{k+1} = b_k + u_{b,k} \Delta t$.

A. Multipath Model

In complicated environments, where reflection surfaces (like exterior walls of buildings) and scatterers (like smaller objects along the road) are common, wireless signals often reflect and scatter before reaching the agent via multiple paths. As NLOS MPCs embed information pertinent to both agent localization and environmental context, we exploit those MPCs to enhance localization accuracy and achieve environment sensing.

In general, NLOS MPCs can be categorized into three types, as shown in Fig. 1: 1) MPCs induced by reflections; 2) MPCs caused by scatterings; and 3) MPCs influenced by both scatterings and reflections. The diverse geometric relationships between the agent and the environment for each MPC type present a significant challenge: identifying these heterogeneous multipaths. This involves determining the specific category to which each MPC belongs. To overcome this deficiency, we introduce a special form of virtual transmitters (VTs), allowing us to treat all types of MPCs in a unified way. Through the lens of VT, all NLOS MPCs can be modeled as if they are virtually emitted from VTs [4] and described as

$$\mathbf{x}_{\text{vt}}^{(l)} = \begin{bmatrix} (\mathbf{r}_{\text{vt}}^{(l)})^T & b_{\text{vt}}^{(l)} \end{bmatrix}^T \quad (3)$$

where $\mathbf{r}_{\text{vt}}^{(l)} = [x_{\text{vt}}^{(l)} \ y_{\text{vt}}^{(l)}]^T \in \mathbb{R}^2$ denote the 2-D position of the l -th VT and $b_{\text{vt}}^{(l)}$ is the additional propagation length of this MPC. Taking the four MPCs in Fig. 1 for illustration:

- 1) The reflection MPC can be viewed as being directly transmitted from the VT which is the anchor's mirror image to the reflector (VT1);
- 2) The MPC induced by a scatterer can be viewed as being directly transmitted from the scatterer $\mathbf{r}_{\text{vt}}^{(2)} := \mathbf{r}_S = [x_S \ y_S]^T$ with an additional propagation bias $b_{\text{vt}}^{(2)} = \|\mathbf{r}_b - \mathbf{r}_S\|_2$ (VT2);

- 3) The MPCs under the dual effect of scattering and reflection can also be viewed as being directly transmitted from a VT with an additional propagation bias. As in Fig. 1, MPCs of VT3 and VT4 are composed of one reflection and one scattering each, albeit in a different sequence. VT3 is located at the scatterer's mirror image to the reflector with $b_{\text{vt}}^{(3)} = \|\mathbf{r}_b - \mathbf{r}_S\|_2$ and VT4 is located at the same location as the scatterer but with $b_{\text{vt}}^{(4)} = \|\mathbf{r}_b - \mathbf{r}_{\text{vt}}^{(3)}\|_2$.

B. Formulating Multipath Components Using RFS

As MPCs emerge and die along with the movement of the agent, and due to clutter and the missed detection phenomena, we need to identify which VTs are present and more importantly, manage the NP-hard data association task for both VTs and observations across various time instances. To address this issue, we group VTs and wireless measurements into sets, instead of the conventional matrices. A random finite set is a finite-set-valued random variable, which is random in both the number of elements and the values of the elements themselves [12]. By adopting the RFS framework, we can more adeptly characterize the stochastic nature of both the detection process and the environment's dynamics for radio-SLAM.

We formulate the map of VTs, which encompasses all detected VTs, as an RFS to accommodate its time-varying characteristics. This set at time instant t_k is denoted by $\mathcal{M}_k = \{\mathbf{m}_k^1, \mathbf{m}_k^2, \dots, \mathbf{m}_k^{|\mathcal{M}_k|}\}$.

Remark 1: The benefits of this VT model are summarized as follows: First, our method enables a consistent description and utilization of all types of MPCs, including those arising from multiple reflections and scatterings. In contrast, other approaches use distinct models for different types of MPCs, necessitating the identification of the MPC type prior to filtering or the usage of multiple filters in the filtering stage. Moreover, these methods are unable to describe MPCs affected by the combined effects of reflections and scatterings. Second, a notable challenge encountered in previous works is the difficulty of distinguishing MPCs whose VTs are located at the same spatial position. This situation often arises when different MPCs undergo the same scatterer before reaching the receiver. An example of this is VT2 and VT4 in Fig. 1. The introduced VT model overcomes this challenge by including the additional propagation bias parameter, as shown in (3), which is distinct for VT2 and VT4, allowing for their differentiation. This feature facilitates the development of the method for accurately discerning environmental characteristics. Moreover, utilizing RFSs, we can explicitly bypass the NP-hard data association step. These advantages highlight the effectiveness and practicality of our VT model in handling complex

propagation environments and leveraging multipath information for improved localization and sensing.

On the other hand, the time-of-arrivals (ToAs) and angle-of-arrivals (AoAs) of detected MPCs are estimated from the channel impulse response (CIR) [6] [13]. Then, the entire set of measurements at time instant t_k under the RFS framework can be described by

$$\mathcal{Z}_k = \{\mathcal{Z}_k^{(0)}, \mathcal{Z}_k^{\text{NLOS}}\} \quad (4)$$

where RFSs $\mathcal{Z}_k^{(0)}$ and $\mathcal{Z}_k^{\text{NLOS}}$ describe the LOS and the NLOS measurements at time instant t_k , respectively, which are non-empty when LOS/NLOS MPCs are detected or false alarms occur, and are empty otherwise, i.e.

$$\mathcal{Z}_k^{(0)} = \begin{cases} \{\mathbf{z}_k^{(0)}\}, & \text{LOS signal detected,} \\ \emptyset, & \text{LOS signal miss,} \end{cases} \quad \mathcal{Z}_k^{\text{NLOS}} = \bigcup_{l \geq 1} \{\mathbf{z}_k^{(l)}\}$$

and the detection probability for a VT m with the agent located at \mathbf{x} is denoted as $P_D(m, \mathbf{x})$.

The range-bearing observation of the l -th NLOS MPC is

$$\mathbf{z}_k^{(l)} = \begin{bmatrix} d_k^{(l)} \\ \theta_k^{(l)} \end{bmatrix} = \begin{bmatrix} \|\mathbf{r}_k - \mathbf{r}_{\text{vt}}^{(l)}\|_2 + b_k + b_{\text{vt}}^{(l)} \\ \arctan\left(\frac{y_{\text{vt}}^{(l)} - y_k}{x_{\text{vt}}^{(l)} - x_k}\right) \end{bmatrix} + \boldsymbol{\omega}_k^{(l)} \quad (5)$$

in which $\boldsymbol{\omega}_k^{(l)}$ denotes the AWGN with standard deviation σ_d and σ_θ for the range and the bearing measurements, respectively. The LOS measurement $\mathbf{z}_k^{(0)}$ has the same structure as that in (5) but with noise standard deviations $\sigma_d^{(0)}$ and $\sigma_\theta^{(0)}$. All the measurements at time instance t_k , including real measurements and clutter are grouped in (4).

To achieve integrated localization and sensing, we aim to simultaneously estimate the agent state \mathbf{x}_k and the VT map \mathcal{M}_k using $\mathcal{Z}_{1:k}$, representing measurements from t_1 to t_k , i.e., computing the posterior probability distribution $p(\mathbf{x}_k, \mathcal{M}_k | \mathcal{Z}_{1:k})$.

III. INTEGRATED LOCALIZATION AND ENVIRONMENT SENSING VIA PHD FILTERING

Our method for estimating the agent state and the VT map includes 4 steps: particle propagation, map prediction, map update and particle reweight/resampling, as shown in Fig. 2.

The computation of $p(\mathbf{x}_k, \mathcal{M}_k | \mathcal{Z}_{1:k})$ using a homogeneous filter is challenging because \mathbf{x}_k is a vector and \mathcal{M}_k is an RFS. To address this problem, we decompose the posterior density based on the Rao-Blackwellisation step in RBPFs

$$p(\mathbf{x}_k, \mathcal{M}_k | \mathcal{Z}_{1:k}) = p(\mathbf{x}_k | \mathcal{Z}_{1:k}) p(\mathcal{M}_k | \mathcal{Z}_{1:k}, \mathbf{x}_k) \quad (6)$$

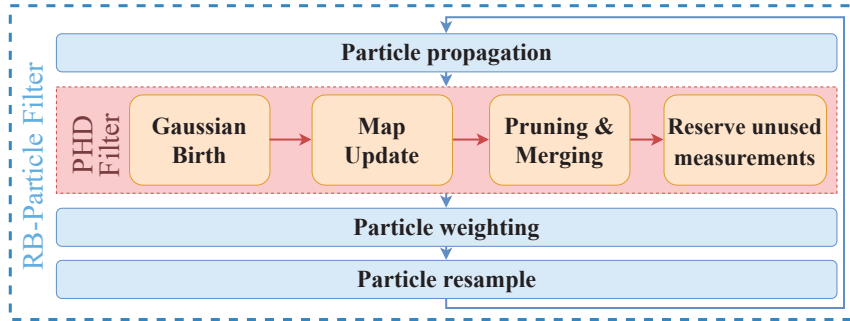


Fig. 2. A General Look at the complete PHD-SLAM algorithm

where the first term on the right-hand side (RHS) is the marginal posterior probability distribution of the agent state \mathbf{x}_k , and the second term is the conditional probability distribution of the VT map \mathcal{M}_k . In this way, we can use a particle filter to sample and describe the agent state \mathbf{x}_k and its marginal distribution. For each particle, given the current agent state related with the particle, we then use a different filter to estimate the RFS VT map \mathcal{M}_k [11], [14], [15]. Moreover, since calculating the posterior probability distribution of RFSs is computational intractable, we adopt a common approach and turn to calculate the first-order statistical moment of the RFS, known as the probability hypothesis density (PHD) [9], [11].

A. Importance Sampling and Particle Propagation

At time instant t_k , N particles are used to describe the agent state \mathbf{x}_k , where the weight of the i -th particle $\mathbf{x}_k^{(i)}$ is denoted as $w_k^{(i)}$. For the i -th particle, we use $v_k^{(i)}(\mathbf{m})$ to describe the corresponding VT map's PHD at \mathbf{m} . Therefore, the particle set at time instant t_k is:

$$\mathcal{P}_k = \{\mathbf{x}_k^{(i)}, v_k^{(i)}(\mathbf{m}), w_k^{(i)}\}_{i=1}^N. \quad (7)$$

Then the posterior probability density function (PDF) of the agent state can be approximated as:

$$p(\mathbf{x}_k | \mathcal{Z}_{1:k}) := p_{k|k}(\mathbf{x}) = \sum_{i=1}^N w_k^{(i)} \delta(\mathbf{x} - \mathbf{x}_k^{(i)}) \quad (8)$$

and we similarly define $p_{k+1|k}(\mathbf{x}) := p(\mathbf{x}_{k+1} | \mathcal{Z}_{1:k})$.

In the particle propagation step at time t_k , particle state $\mathbf{x}_{k|k-1}^{(i)}$ and weight $w_{k|k-1}^{(i)}$ are predicted based on the principle of importance sampling [16], we use the importance density $q(\mathbf{x}_k^{(i)} | \mathbf{x}_{k-1}^{(i)}, \mathcal{Z}_k)$ to sample particle states, which satisfies

$$q(\mathbf{x}_k^{(i)} | \mathcal{Z}_{1:k}) = q(\mathbf{x}_k^{(i)} | \mathbf{x}_{k-1}^{(i)}, \mathcal{Z}_k) q(\mathbf{x}_{k-1}^{(i)} | \mathcal{Z}_{1:k-1}) \quad (9)$$

and calculate predicted particle weight $w_{k|k-1}^{(i)}$ by

$$w_{k|k-1}^{(i)} \propto w_{k-1|k-1}^{(i)} \frac{p(\mathbf{x}_k^{(i)} | \mathbf{x}_{k-1}^{(i)})}{q(\mathbf{x}_k^{(i)} | \mathbf{x}_{k-1}^{(i)}, \mathcal{Z}_k)}. \quad (10)$$

Similar to the widely adopted approach in [9], [11], [14], [17], [18], we use the motion model to characterise the importance density. Specifically, we use $q(\mathbf{x}_k^{(i)} | \mathbf{x}_{k-1}^{(i)}, \mathcal{Z}_k) = p(\mathbf{x}_k^{(i)} | \mathbf{x}_{k-1}^{(i)})$ to simplify calculations, which yields $w_{k|k-1}^{(i)} = w_{k-1|k-1}^{(i)}$.

B. PHD Filtering

Next, we address each particle's VT map individually. For the posterior PHD of the VT map for the i -th particle at time instant t_k , we model it using a Gaussian-mixture (GM) form:

$$v_{k|k}^{(i)}(\mathbf{m}) = \sum_{j=1}^{M_{k|k}^{(i)}} \alpha_{k|k,j}^{(i)} \mathcal{N}(\mathbf{m}; \boldsymbol{\mu}_{k|k,j}^{(i)}, \mathbf{C}_{k|k,j}^{(i)}) \quad (11)$$

where $M_{k|k}^{(i)}$ is the number of Gaussian components (GCs) in the GM. To obtain the PHD of the VT map at time t_{k+1} , we iterate over two steps: prediction and update.

1) *PHD Prediction with MPCs' Birth and Death*: In complex propagation environments, MPCs emerge and die along with the movement of the agent. Thus, changeable VTs require special consideration when designing the PHD filter. Although traditional GM-PHD filters generate birth GCs using static birth models, it has been shown that generating birth GCs directly from measurements achieves better performance [18], as is adopted in various works including [5], [11], [18], [19]. Here, we propose a new method for our VT model to generate birth GCs according to NLOS measurements that do not match with any pre-existing VTs identified in the previous iteration.

As shown in Fig. 3, for particle i , suppose there are $B_k^{(i)}$ NLOS measurements that do not match with any existing VTs at time instant t_{k-1} . To simplify the notations, suppose that the l -th unmatched NLOS measurement has the value of $\mathbf{z}_{B_k,l} = [d, \theta]^T$, we generate a birth GC with respect to this measurement, taking the form:

$$v_{B_k,l}^{(i)}(\mathbf{m}) = \mathcal{N}(\mathbf{m}; \boldsymbol{\mu}_{B_k,l}^{(i)}, \mathbf{C}_{B_k,l}^{(i)})$$

and initialize the mean $\boldsymbol{\mu}_{B_k,l}^{(i)} = [(\mathbf{r}_{B_k,l}^{(i)})^T \mathbf{b}_{B_k,l}^{(i)}]^T$ and covariance $\mathbf{C}_{B_k,l}^{(i)}$ by the measurement \mathbf{z} as follows:

First, in case of the birth GC's mean $\boldsymbol{\mu}_{B_k,l}^{(i)}$, with angle measurement θ , we set $\mathbf{r}_{B_k,l}^{(i)}$ to the same direction relative to the agent state as θ . With range measurement d , we have:

$$\|\mathbf{r}_{k-1}^{(i)} - \mathbf{r}_{B_k,l}^{(i)}\|_2 + b_{B_k,l}^{(i)} + b_{k-1}^{(i)} = d \quad (12)$$

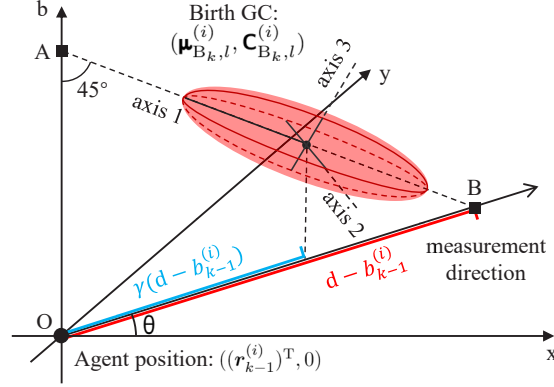


Fig. 3. For the i -th particle with state $\mathbf{x}_k^{(i)}$ at time instant t_k , parameters of the birth GC $(\boldsymbol{\mu}_{B_{k,l}}^{(i)}, \mathbf{C}_{B_{k,l}}^{(i)})$ is generated according to the measurement $\mathbf{z}_{B_{k,l}} = [d, \theta]^T$ and the particle state $\mathbf{x}_{k-1}^{(i)}$. $\boldsymbol{\mu}_{B_{k,l}}^{(i)}$ is constrained on the line AB. axis 1,2,3 are the three main axes of the GC's confidence ellipsoid, where axis 1 is set along line AB and axis 3 is set within plane OAB.

due to the unknown additional propagation bias $b_{B_{j,k}}^{(i)}$, $\mathbf{r}_{B_{k,j}}^{(i)}$ still has ambiguity, to address this issue, we introduce parameter γ ($0 \leq \gamma \leq 1$), where

$$\|\mathbf{r}_{k-1}^{(i)} - \mathbf{r}_{B_{k,l}}^{(i)}\|_2 = \gamma(d - b_{k-1}^{(i)}) \quad (13)$$

which allows us to control the mean of birth GC by γ .

Second, in case of the GC's covariance $\mathbf{C}_{B_{k,l}}^{(i)}$, we set:

$$\mathbf{C}_{B_{k,l}}^{(i)} = \mathbf{T}(\theta) \boldsymbol{\Sigma}(d) \mathbf{T}(\theta)^T \quad (14)$$

where $\mathbf{T}(\theta)$ is a three-dimension rotational matrix, given by

$$\mathbf{T}(\theta) = \begin{bmatrix} \frac{\cos(\theta)}{\sqrt{2}} & -\sin(\theta) & \frac{\cos(\theta)}{\sqrt{2}} \\ \frac{\sin(\theta)}{\sqrt{2}} & \cos(\theta) & \frac{\sin(\theta)}{\sqrt{2}} \\ -\frac{1}{\sqrt{2}} & 0 & \frac{1}{\sqrt{2}} \end{bmatrix} \quad (15)$$

and $\boldsymbol{\Sigma}(d)$ is a diagonal matrix depended on distance d by $[\boldsymbol{\Sigma}(d)]_{11} = \zeta \cdot (d - b_{k-1}^{(i)})^2$, $[\boldsymbol{\Sigma}(d)]_{22} = \iota \cdot (d - b_{k-1}^{(i)})^2 (\sigma_\theta)^2$ and $[\boldsymbol{\Sigma}(d)]_{33} = \xi \cdot (\sigma_d)^2$ with user-defined non-negative parameters ζ , ι , and ξ . $[\boldsymbol{\Sigma}(d)]_{11}$, $[\boldsymbol{\Sigma}(d)]_{22}$, $[\boldsymbol{\Sigma}(d)]_{33}$ denote the variance of the birth GC along axis 1,2 and 3 in Fig. 3 respectively.

After deciding birth GCs, we predict map PHD $v_{k|k-1}^{(i)}(\mathbf{m})$ according to posterior map PHD

and birth GCs by

$$\begin{aligned}
v_{k|k-1}^{(i)}(\mathbf{m}) &= v_{k-1|k-1}^{(i)}(\mathbf{m}) + \sum_{l=1}^{B_k^{(i)}} \alpha_B \mathcal{N}(\mathbf{m}; \boldsymbol{\mu}_{B_k,l}^{(i)}, \mathbf{C}_{B_k,l}^{(i)}) \\
&= \sum_{j=1}^{M_{k|k-1}^{(i)}} \alpha_{k|k-1,j}^{(i)} \mathcal{N}(\mathbf{m}; \boldsymbol{\mu}_{k|k-1,j}^{(i)}, \mathbf{C}_{k|k-1,j}^{(i)})
\end{aligned} \tag{16}$$

where α_B is the GC's birth weight.

2) *PHD Update*: With wireless measurements at time t_k , we then update the PHD map of each particle. For particle i , denoting $P_D(\boldsymbol{\mu}_{k|k-1,j}^{(i)}, \mathbf{x}_k^{(i)})$ as $P_{D,k,j}^{(i)}$, the posterior PHD is updated according to the PHD filter corrector equation [14]:

$$\begin{aligned}
v_{k|k}^{(i)}(\mathbf{m}) &= \sum_{l=1}^{|\mathcal{Z}_k^{\text{NLOS}}|} \sum_{j=1}^{M_{k|k-1}^{(i)}} \alpha_{k,l,j}^{(i)} \mathcal{N}(\mathbf{m}; \boldsymbol{\mu}_{k,l,j}^{(i)}, \mathbf{C}_{k,l,j}^{(i)}) \\
&+ \sum_{j=1}^{M_{k|k-1}^{(i)}} (1 - P_{D,k,j}^{(i)}) \alpha_{k|k-1,j}^{(i)} \mathcal{N}(\mathbf{m}; \boldsymbol{\mu}_{k|k-1,j}^{(i)}, \mathbf{C}_{k|k-1,j}^{(i)})
\end{aligned} \tag{17}$$

where the second term is induced by missed detections. For the first term, $\boldsymbol{\mu}_{k,l,j}^{(i)}$ and $\mathbf{C}_{k,l,j}^{(i)}$ are the mean and variance of the j -th GC corrected by the l -th measurement in $\mathcal{Z}_k^{\text{NLOS}}$ using extended kalman filters (EKFs) [9]. Moreover, we model clutter as a Poisson point process with intensity $\kappa(\mathbf{z})$ and the expected number of clutter as λ_c . The corrected GCs' weights can be updated like a common PHD filter as in [9], [11]:

$$\alpha_{k,l,j}^{(i)} = \frac{P_{D,k,j}^{(i)} \alpha_{k|k-1,j}^{(i)} q_{k,j}^{(i)}(\mathbf{z}_k^{(l)})}{\kappa(\mathbf{z}_k^{(l)}) + \sum_{s=1}^{M_{k|k-1}^{(i)}} P_{D,k,j}^{(i)} \alpha_{k|k-1,s}^{(i)} q_{k,s}^{(i)}(\mathbf{z}_k^{(l)})} \tag{18}$$

where $q_{k,j}^{(i)}(\mathbf{z}_k^{(l)})$ is the probability density of the l -th measurement related with the j -th VT GC. At the end of the update step, measurements that do not match with any VTs are reserved to generate birth GCs in the next PHD filtering iteration, as shown in Fig. 2 and mentioned in Section III-B1.

C. Particle Reweight and Resample

Combing the updated VT map and agent state, we have:

$$\begin{aligned}
p_{k|k}(\mathbf{x}) &\propto p(\mathbf{x}_k, \mathcal{Z}_k | \mathcal{Z}_{1:k-1}) \\
&= p(\mathcal{Z}_k | \mathbf{x}_k, \mathcal{Z}_{1:k-1}) p_{k|k-1}(\mathbf{x}).
\end{aligned} \tag{19}$$

The updated particle weight for particle i is thus given by

$$\begin{aligned} w_{k|k}^{(i)} &\propto p(\mathcal{Z}_k | \mathbf{x}_k^{(i)}, \mathcal{Z}_{1:k-1}) w_{k|k-1}^{(i)} \\ &= p(\mathcal{Z}_k^{(0)} | \mathbf{x}_k^{(i)}) p(\mathcal{Z}_k^{\text{NLOS}} | \mathbf{x}_k^{(i)}, \mathcal{Z}_{1:k-1}) w_{k|k-1}^{(i)} \end{aligned} \quad (20)$$

where the first term is the contribution of the LOS MPC and is set equal for all particles if LOS measurement is lost. As shown in [11], the second term comes from the NLOS MPCs and satisfies

$$\begin{aligned} p(\mathcal{Z}_k^{\text{NLOS}} | \mathbf{x}_k^{(i)}, \mathcal{Z}_{1:k-1}) &= \\ p(\mathcal{Z}_k^{\text{NLOS}} | \mathbf{x}_k^{(i)}, \Lambda_k) \frac{p(\Lambda_k | \mathbf{x}_k^{(i)}, \mathcal{Z}_{1:k-1})}{p(\Lambda_k | \mathbf{x}_k^{(i)}, \mathcal{Z}_{1:k})} \end{aligned} \quad (21)$$

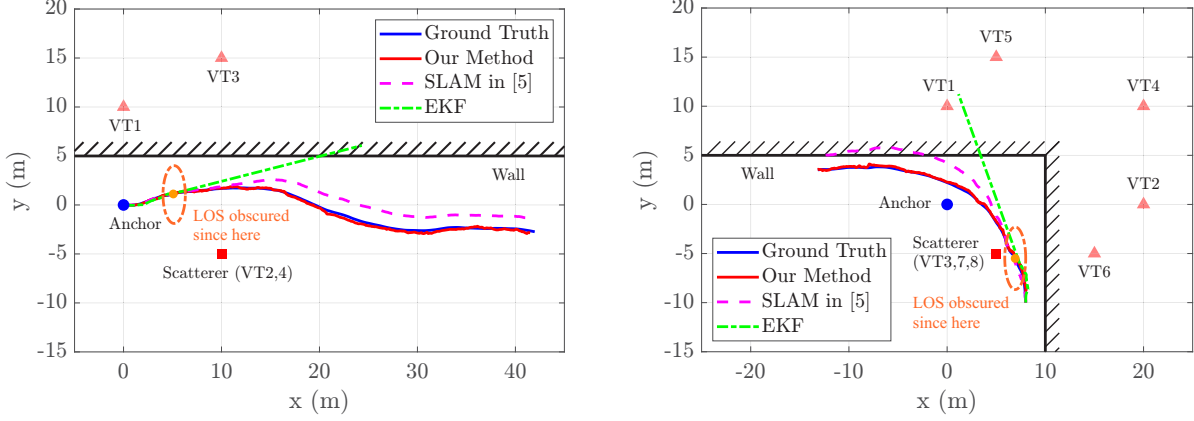
where Λ_k is a free variable. Multiple strategies exist considering the choice of Λ_k , including empty-set strategy, single-feature strategy and multi-feature strategy [11]. To generate more accurate estimates, we adopt the multi-feature strategy to decide Λ_k , as shown in [11], [20]. When the number of effective particles is low, particle resampling will be executed.

Finally, the agent's state and the VT map are estimated using minimum-mean-square-error (MMSE) and maximum-a-posteriori (MAP) estimation respectively. The estimated VT parameters are decided by GCs parameters in the PHD map.

IV. NUMERICAL RESULTS

In this section, two distinct simulation scenarios are investigated, with the layouts of their respective environments illustrated in Fig. 4(a) and Fig. 4(b). In the first scenario, shown in 4(a), there are a base station, a point scatterer, and a planar wall, located at $(0, 0)\text{m}$, $(10, -5)\text{m}$, and along $y = 10\text{m}$, respectively. This configuration will lead to four NLOS MPCs and four corresponding VTs.² The second scenario, depicted in Fig. 4(b), presents a more complex propagation environment. It includes a base station, a point scatterer and two vertical walls, which are located at $(0, 0)\text{m}$, $(5, -5)\text{m}$, and along $y = 5\text{m}$ and $x = 10\text{m}$ for two vertical walls, respectively. This setup results in 8 VTs. We also consider the agent's field of view (FoV), which contributes to a more realistic representation of the real-life scenario. VTs located beyond the agent's FoV distance are not detected, aligning with practical limitations.

²While our method can handle MPCs with any combination of reflections and scatterings, in our simulations, we only consider NLOS MPCs related with either up to two reflections, two scatterings, or a combination of one reflection and one scattering.



(a) Scenario 1: VT1 with 1 reflection, VT2 with 1 scattering, VT3 and VT4 with 1 reflection and 1 scattering.

(b) Scenario 2: VT1 and VT2 with 1 reflection, VT3 with 1 scattering, VT4 with 2 reflections, VT5, VT6, VT7 and VT8 with 1 reflection and 1 scattering.

Fig. 4. Configurations of 2 simulation scenarios and the localization results of one representative experiment of three methods for each scenario.

In both simulation scenarios, the simulation time is set to 30 seconds with the measurement update frequency at 12.5Hz. To assess validity in challenging propagation environments, the LOS measurements only exist in the first 6 seconds. We generate ground truth trajectories using the motion model in (2), where the motion parameters are $\sigma_x = \sigma_y = 0.5m/s^2$. Each trajectory undergoes 10 repetitions, during which distinct MPC measurements are generated using the measurement model in Section II-B for each repetition. Measurement noise parameters are set to $\sigma_d = 0.3m$, $\sigma_\theta = 4 \text{ deg}$ and $\sigma_d^{(0)} = 0.05m$, $\sigma_\theta^{(0)} = 2 \text{ deg}$, with $P_{D,k,j}^{(i)} = 0.95$ within a fixed-range FoV for the agent and $\lambda_c = 0.02$. For the filter setup, we set the particle number to $N = 100$. The filter parameters associated with the measurement model and motion model, including the particles' initial states, align with those employed in the data generation step, and we set the noise parameter for the clock bias as $\sigma_b = 0.01m/s$. For birth GCs' parameters we discussed in (13) and (14) in Section III-B1, we set $\gamma = 0.7$, $\zeta = 0.1$, $\nu = 0.5$, $\xi = 0.3$ and $\alpha_B = 0.01$. Specifically, in the first scenario, utilizing 10 trajectories and 100 simulations, the agent's initial position and velocity are $(0,0)m$ and $(1,0)m/s$ respectively with $b_k = 0.3m$. In particular, the agent's FoV is 60m. In the second scenario, with 5 trajectories and 50 simulations, the agent's initial state and velocity are set to $(8, -10)m$ and $(0,1)m/s$, $b_k = 0.3m$, and the agent's FoV is 30m.

To evaluate the effectiveness of our method, we compare it with the approach presented in

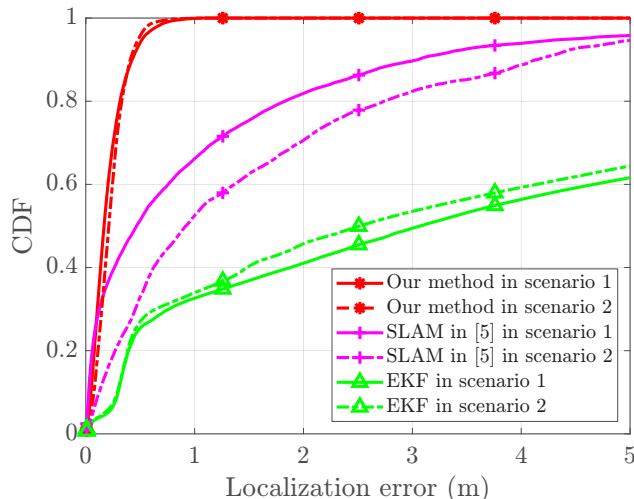


Fig. 5. The cumulative distribution function (CDF) of localization errors of three methods in two scenarios.

[5], where two different PHD filters are used for handling the reflection and scattering MPCs separately. We also compare our method with an EKF-based method that only utilizes LOS measurements as a performance baseline. The parameters in these methods also align with those employed in the data generation step. The estimated trajectories from one experiment are visualized in Fig. 4. The CDF of the localization error across all simulation runs is shown in Fig. 5 and the root mean squared errors (RMSEs) of all VTs' 2-D position estimates are summarized in Tables I and II. The time complexity of our method and the SLAM in [5] at time instant t_k are comparable, both in the order of $\mathcal{O}(N_k \times |\mathcal{M}_k| \times |\mathcal{Z}_k^{\text{NLOS}}|)$.

Fig. 4 and 5 demonstrate the notably enhanced localization accuracy achieved by our method in both scenarios. In the first scenario, our method achieves a localization accuracy with an RMSE of $0.26m$, which is 88.3% better than the SLAM approach in [5] with an RMSE= $2.22m$. It also outperforms the EKF baseline, which has an RMSE of $7.80m$, by 96.1%. Similarly, in the second scenario, our method's RMSE of $0.27m$ surpasses that of the SLAM in [5] (RMSE $2.29m$) by 88.2% and exceeds the EKF baseline (RMSE $8.03m$) by 96.6%. Compared with other methods, Fig. 4 also shows the robustness of our method in scenarios where the LOS path is obscured. This further demonstrates the robustness and superior performance of our method in complex multipath scenarios with a limited FoV, particularly in rapidly changing, LOS-obscured environments with clutter and missed detection.

In terms of environmental sensing, our method excels in achieving significantly higher esti-

TABLE I
THE RMSES OF VT ESTIMATES IN SCENARIO 1

| Method | VT1 (m) | VT2 (m) | VT3 (m) | VT4 (m) |
|-------------|---------|---------|---------|---------|
| Ours | 0.48 | 0.43 | 0.69 | 0.54 |
| SLAM in [5] | 1.96 | 7.36 | 8.96 | 7.36 |

TABLE II
THE RMSES OF VT ESTIMATES IN SCENARIO 2

| Method | VT1 (m) | VT2 (m) | VT3 (m) | VT4 (m) |
|-------------|---------|---------|---------|---------|
| Ours | 1.90 | 1.15 | 0.23 | 1.22 |
| SLAM in [5] | 2.20 | 1.59 | 1.62 | 2.66 |
| Method | VT5 (m) | VT6 (m) | VT7 (m) | VT8 (m) |
| Ours | 2.42 | 0.46 | 0.24 | 0.24 |
| SLAM in [5] | 6.96 | 5.65 | 5.99 | 5.99 |

mation accuracy for every VT in both scenarios, as demonstrated in Table I and II. Moreover, the sensing performance of our method is comparable with its localization accuracy in both simulation scenarios. In contrast, the radio-SLAM method in [5] cannot handle VTs influenced by both reflections and scatterings. As a result, it yields less accurate estimates for VT3 and VT4 in scenario 1, and for VT5, VT6, VT7, and VT8 in scenario 2.³

V. CONCLUSIONS

In this paper, we delivered high-accuracy localization and environmental sensing in an efficient and robust manner. The key to our method is the unified characterization and utilization of

³In Table I, VT2 and VT4 achieve identical RMSEs for the SLAM method in [5], a method that considers only the 2-D positions of VTs. Since VT2 and VT4 share the same positions, this makes them indistinguishable, and thus they have an equal RMSE.

In Table II, VT7 and VT8 have identical RMSEs, while VT3 exhibits a different RMSE for the SLAM method in [5]. The reasons are two-fold. Firstly, VT7 and VT8 are essentially identical in terms of VT, sharing both the same positions and propagation biases. Thus, in the GM-PHD map, VT7 and VT8 are represented by a single GC with a combined weight close to 2. Secondly, the GC corresponding to VT3 has a weight close to 1, distinctly separating it from VT7 and VT8 in the GM-PHD representation.

different types of MPCs via an RFS, which enables us to forge the requirement of identifying MPC types prior to filtering and eliminates the necessity for employing multiple MPC tracking filters. Moreover, our method also can handle MPCs influenced by both reflections and scatterings. The simulation results demonstrated that our method excels in both robustness and effectiveness, particularly in complex environments where the LOS MPC is obscured and in situations involving clutter and missed detections of MPC measurements.

REFERENCES

- [1] M. Z. Win, Y. Shen, and W. Dai, "A theoretical foundation of network localization and navigation," *Proc. IEEE*, vol. 106, no. 7, pp. 1136–1165, Jul. 2018.
- [2] H. Zhao, N. Zhang, and Y. Shen, "Beamspace direct localization for large-scale antenna array systems," *IEEE Trans. Signal Process.*, vol. 68, pp. 3529–3544, May 2020.
- [3] T. Deißler and J. Thielecke, "UWB SLAM with Rao-Blackwellized Monte Carlo data association," in *Proc. Int. Conf. on Indoor Positioning and Navigation*, Sep. 2010, pp. 1–5.
- [4] C. Gentner, T. Jost, W. Wang, S. Zhang, A. Dammann, and U. C. Fiebig, "Multipath assisted positioning with simultaneous localization and mapping," *IEEE Trans. Wireless Commun.*, vol. 15, no. 9, pp. 6104–6117, Sep. 2016.
- [5] H. Kim, K. Granström, L. Gao, G. Battistelli, S. Kim, and H. Wymeersch, "5G mmWave cooperative positioning and mapping using multi-model PHD filter and map fusion," *IEEE Trans. Wireless Commun.*, vol. 19, no. 6, pp. 3782–3795, Jun. 2020.
- [6] T. Wang, J. Liu, and Y. Shen, "A robust single-anchor localization method with multipath assistance in NLOS environments," in *Proc. IEEE Global Commun. Conf.*, Madrid, Spain, Dec. 2021, pp. 1–6.
- [7] H. Kim, H. Chen, M. F. Keskin, Y. Ge, K. Keykhosravi, G. C. Alexandropoulos, S. Kim, and H. Wymeersch, "RIS-enabled and access-point-free simultaneous radio localization and mapping," *IEEE Trans. Wireless Commun.*, Aug. 2023.
- [8] Z. Yang, H. Zhang, H. Zhang, B. Di, M. Dong, L. Yang, and L. Song, "MetaSLAM: Wireless simultaneous localization and mapping using reconfigurable intelligent surfaces," *IEEE Trans. Wireless Commun.*, vol. 22, no. 4, pp. 2606–2620, Apr. 2022.
- [9] J. Mullane, B.-N. Vo, M. D. Adams, and B.-T. Vo, "A random-finite-set approach to Bayesian SLAM," *IEEE Trans. Robot.*, vol. 27, no. 2, pp. 268–282, Apr. 2011.
- [10] B. Amjad, Q. Z. Ahmed, P. I. Lazaridis, M. Hafeez, F. A. Khan, and Z. D. Zaharis, "Radio SLAM: A review on radio-based simultaneous localization and mapping," *IEEE Access*, vol. 11, pp. 9260–9278, Jan. 2023.
- [11] K. Y. Leung, F. Inostroza, and M. Adams, "Multifeature-based importance weighting for the phd slam filter," *IEEE Trans. Aerosp. Electron. Syst.*, vol. 52, no. 6, pp. 2697–2714, Dec. 2016.
- [12] B. T. Vo, "Random finite sets in multi-object filtering," Ph.D. dissertation, School of Electrical, Electronic and Computer Engineering, The University of Western Australia, Australia, 2008.
- [13] H. Zhao, M. Huang, and Y. Shen, "High-accuracy localization in multipath environments via spatio-temporal feature tensorization," *IEEE Trans. Wireless Commun.*, vol. 21, no. 12, pp. 10 576–10 591, Dec. 2022.
- [14] M. Vihola, "Rao-blackwellised particle filtering in random set multitarget tracking," *IEEE Trans. Aerosp. Electron. Syst.*, vol. 43, no. 2, pp. 689–705, Jun. 2007.
- [15] K. Murphy and S. Russell, "Rao-blackwellised particle filtering for dynamic bayesian networks," in *Sequential Monte Carlo methods in practice*. Springer, 2001, pp. 499–515.

- [16] N. Bergman, "Recursive bayesian estimation: Navigation and tracking applications," Ph.D. dissertation, Linköping University, May 1999.
- [17] M. S. Arulampalam, S. Maskell, N. Gordon, and T. Clapp, "A tutorial on particle filters for online nonlinear/non-gaussian bayesian tracking," *IEEE Trans. Signal Process.*, vol. 50, no. 2, pp. 174–188, Feb. 2002.
- [18] J. Houssineau and D. Laneuville, "PHD filter with diffuse spatial prior on the birth process with applications to gm-phd filter," in *Int. Conf. Inf. Fusion*, Edinburgh, UK, Jul. 2010, pp. 1–8.
- [19] L. Gao, G. Battistelli, and L. Chisci, "PHD-SLAM 2.0: Efficient SLAM in the presence of misdetections and clutter," *IEEE Trans. Robot.*, vol. 37, no. 5, pp. 1834–1843, Oct. 2021.
- [20] K. Y. K. Leung, F. Inostroza, and M. Adams, "An improved weighting strategy for rao-blackwellized probability hypothesis density simultaneous localization and mapping," in *Proc. Int. Conf. on Control, Autom. and Inf. Sci.*, 2013, pp. 103–110.